Recombination rate variation shapes genomic variability of phylogeographic structure in a widespread North American songbird (Aves: *Certhia americana*)

Joseph D. Manthey[1]*, Garth M. Spellman[2]

[1]Department of Biological Sciences, Texas Tech University. Lubbock, Texas, USA.

[2]Department of Zoology, Denver Museum of Nature & Science, Denver, Colorado, USA.

*Corresponding author: jdmanthey@gmail.com

Running head: Recombination rate variation shapes phylogeographic structure variation

ABSTRACT

The nonrandom distribution of chromosomal characteristics and functional elements—genomic architecture—impacts the relative strengths and impacts of population genetic processes across the genome. Due to this relationship, genomic architecture has the potential to shape variation in population genetic structure across the genome. Population genetic structure has been shown to vary across the genome in a variety of taxa, but this body of work has largely focused on pairwise population genomic comparisons between closely related taxa. Here, we used whole genome sequencing of seven phylogeographically structured populations of a North American songbird, the Brown Creeper (*Certhia americana*), to determine the impacts of genomic architecture on phylogeographic structure variation across the genome. Using multiple methods to infer phylogeographic structure—ordination, clustering, and phylogenetic methods—we found that recombination rate variation explained a large proportion of phylogeographic structure variation. Genomic regions with low recombination showed phylogeographic structure consistent with the genome-wide pattern. In regions with high recombination, we found strong phylogeographic structure, but with discordant patterns relative to the genome-wide pattern. In regions with high recombination rate, we found that populations with small effective population sizes evolve relatively more rapidly than larger populations, leading to discordant signatures of phylogeographic structure. These results suggest that the interplay between recombination rate variation and effective population sizes shape the relative impacts of linked selection and genetic drift in different parts of the genome. Overall, the combined interactions of population genetic processes, genomic architecture, and effective population sizes shape patterns of variability in phylogeographic structure across the genome of the Brown Creeper.

Keywords: phylogeography, population genomics, genetic architecture, demography

INTRODUCTION

The formation of population structure is implicit in the speciation process (Allmon, 1992; Mayr et al., 1963). Speciation is a continuum; early differentiating populations may have few genomic regions with evidence for genetic differentiation or barriers to gene flow (Ellegren et al., 2012; Nosil and Feder, 2012; Toews et al., 2016; Wu, 2001) while later in the speciation process two diverging populations may exhibit strong genetic differentiation across their entire genomes (Nosil and Feder, 2012; Ravinet et al., 2018; Wu, 2001). Across the genome, variation in local evolutionary history is shaped by the relative strengths of the population genomic processes of natural selection, gene flow, and genetic drift. For example, population genetic structure may differ in genomic regions with strong natural selection or differential patterns of gene flow relative to the rest of the genome (Louis et al., 2020; Whiting et al., 2021).

Variable impacts of selection, drift, and gene flow across the genome may be partially attributed to genomic architecture—the nonrandom distribution of chromosomal characteristics and functional elements (Koonin, 2009)—whereby variation in gene content, recombination rates, or other genomic characteristics impact the relative effects of population genomic processes. For example, we expect that genomic regions with lower recombination rates will be relatively depleted of genetic diversity and genetic differentiation will accumulate faster, due to relatively increased effects of linked selection (Cruickshank and Hahn, 2014; Haenel et al., 2018; Hey and Kliman, 2002; Nachman and Payseur, 2012). Indeed, speciation and population genomic studies have often found a negative relationship between recombination rates and genetic differentiation across the genome (Kulathinal et al., 2008; Manthey et al., 2021; Roesti et al., 2013; Stankowski et al., 2019; Vijay et al., 2016).

If genomic architecture impacts population genomic patterns within populations and between pairs of taxa, we may naturally extend this idea to phylogeographic patterns in taxa with multiple lineages at different stages of evolutionary distinctiveness. As such, we may

predict that estimates of phylogeographic structure will vary across the genome and be shaped by several factors and their interactions: (1) population size variation of differentiating populations shaping relative strengths of selection and drift, (2) time since divergence began, (3) genomic architecture, and (4) quantity of interpopulation gene flow. Exemplar taxa to better understand the impacts of genomic architecture on population genetic structure are species (or species complexes) with multiple lineages on distinct evolutionary trajectories, populations with different effective sizes, and genomes exhibiting heterogeneous genomic architecture.

The Brown Creeper (*Certhia americana*) is an excellent study organism to understand the impacts of genomic architecture on phylogeographic structure; its genome is highly heterogeneous in both structure and content, and it has seven distinct phylogeographic lineages (Manthey et al., 2011a; Manthey et al., 2015). The genome of the Brown Creeper, as like other birds, has chromosomes that (1) span two orders of magnitude in size, (2) vary in their gene and repetitive element content, and (3) exhibit local effective recombination rates that can vary by an order of magnitude or more (Dutoit et al., 2017; Ellegren, 2010; Kapusta and Suh, 2017; Kawakami et al., 2014; Manthey et al., 2021). Additionally, the Brown Creeper has strong phylogeographic structure, with two main lineages that have been diverging around one million years (Fig. 1A), multiple phylogeographically structured clades within each of these two main lineages, and populations with different effective sizes (Manthey et al., 2011a, b; Manthey et al., 2015, 2021).

Using the Brown Creeper as our study taxon, we used whole-genome sequencing data to assess how genome architecture influences phylogeographic structure; we used phylogenetic, ordination, and population genetic clustering methods to characterize phylogeographic structure across the genome. Our aims here were twofold. First, we looked to decipher how genomic architecture and effective population sizes shape phylogeographic structure variation across the genome. Second, because phylogeographic structure may be

104 estimated in many ways, we wanted to identify whether phylogeographic signal variation was
105 consistent using different methodologies.

106 Based on previous population genomic research, we hypothesized that genomic regions
107 with low recombination rates will have faster lineage sorting. Based on this hypothesis, we
108 would predict that phylogeographic estimates consistent with the species or population level
109 evolutionary history of the group will be concentrated in genomic regions with low
110 recombination. Additionally, we may predict a couple alternative patterns in high recombination
111 regions. We may identify mixed or weak phylogeographic structure in high recombination
112 regions. Alternatively, we may identify strong, but divergent patterns of phylogeographic
113 structure in high recombination regions linked with varied molecular evolutionary rates among
114 sampled populations. We may also predict an interaction between recombination rate and
115 population sizes; whereby, relatively smaller populations will undergo faster molecular evolution
116 in genomic regions characterized by stabilizing selection, such as in gene-dense, high
117 recombination genomic regions.
118
119 **MATERIALS AND METHODS**
120
121 ***Study organism, sampling, and sequencing.*** The Brown Creeper is a songbird found in
122 forested regions of the Americas; it has a widespread distribution ranging from Honduras in the
123 south to Alaska in the north (Fig. 1A) (Poulin et al., 2020). The Brown Creeper is aptly named; it
124 creeps up trees in search of its largely invertebrate diet and has dark coloration on its back and
125 sides (Fig. 1A inset) that makes for excellent camouflage on trees with dark bark. In previous
126 work using tens to thousands of genetic markers, we have identified phylogeographic structure
127 in the Brown Creeper, with up to seven distinct lineages (Manthey et al., 2011a, b; Manthey et
128 al., 2015). Here, we aimed to obtain population genomic sequencing data for seven populations
129 with three individuals sampled per population (Fig 1, Table S1). We downloaded previously

published sequencing data from two of these populations and one outgroup sample of *C. familiaris* (Table S1) (Manthey et al., 2021). For the other five populations, we obtained representative tissue samples from natural history museums and extracted genomic DNA using QIAGEN DNeasy blood and tissue kits following manufacturer guidelines. DNA from extractions was used to create standard Illumina sequencing libraries, followed by sequencing on an Illumina NovaSeq6000 at the Texas Tech University Center for Biotechnology and Genomics with the goal of obtaining ~15-30× coverage per individual.

Reference genome and genomic architecture. For the reference genome, we used the chromosome-scale *Certhia americana* genome we assembled for a prior study (NCBI assembly ASM1869719v1; Manthey et al. 2021). From data reported in this previous study (Manthey et al. 2021), we summarized mean effective recombination rates for each of the two main Brown Creeper lineages, transposable element (TE) and gene density, and GC content across the genome in 50kbp and 100 kbp non-overlapping sliding windows (Fig. 2). We used the mean effective recombination rates of the two lineages because they were highly correlated ($r = 0.829$-0.861 across different correlation metrics; all $p << 0.001$), and we can assume relatively conserved recombination rates over short evolutionary time frames (Singhal et al., 2015). Briefly, these estimates were initially obtained with the following methods: effective recombination rate was estimated using LDhat (McVean and Auton, 2007), TEs were annotated with RepeatMasker v4.08 (Smit et al., 2015), and gene content was annotated with MAKER v2.31.10 (Cantarel et al., 2008).

Sequencing data filtering and genotyping. We used the program bbduk (Bushnell, 2014) to quality filter raw sequencing data. We then use BWA v0.7.17 (Li and Durbin, 2009) to align filtered reads to the *Certhia americana* reference genome. Next, we used samtools v1.4.1 (Li et al., 2009) to convert the BWA output SAM file to BAM format, followed by using the Genome

Analysis Toolkit (GATK) v4.1.0.0 (McKenna et al., 2010) to clean, sort, add read groups to, and remove duplicates from BAM files. We used the samtools 'depth' command to measure sequencing coverage across the reference genome for each individual (Fig. S1, Table S1).

We then used GATK in three steps to genotype all individuals: we used the 'HaplotypeCaller' function to call preliminary genotypes for each individual, built a database for all samples using the 'GenomicsDBImport' function, and lastly used the 'GenotypeGVCFs' function to group genotype all individuals together for both variant and invariant sites. We filtered the genotype data using VCFtools v0.1.14 (Danecek et al., 2011) with the following restrictions: (1) minimum site quality of 20, (2) minimum genotype quality of 20, (3) minimum depth of coverage of 6, (4) maximum mean depth of coverage of 50, and (5) removal of indels. For downstream analyses, we used various settings for (1) amount of missing data allowed, (2) whether the outgroup was included, (3) inclusion or exclusion of invariant sites, and (4) thinning between sites (see Table 1 for exact dataset characteristics used for all seven datasets used for analyses). Although it has been suggested that variation in minor allele frequency (MAF) filtering may impact estimates of genetic structure (Linck and Battey, 2019), we did not filter for a minimum MAF because we previously showed that changing MAF did not significantly impact pairwise F_{ST} calculations in *C. americana* (Manthey et al., 2021).

Phylogenomics. We estimated "gene trees" in non-overlapping windows (window size 50 kbp and 100 kbp; datasets C and D in Table 1) using RaxML v8.2.12 (Stamatakis, 2014) with the GTRCAT model of sequence evolution. For a window to be included, we required a minimum of 10 kbp in the alignment following filtering. This resulted in 19,639 phylogenies for the 50 kbp sliding windows and 9846 phylogenies for the 100 kbp sliding windows. We summarized the best-supported trees using the sumtrees.py script, part of the DendroPy Python package (Sukumaran and Holder, 2010). Lastly, we used ASTRAL III v 5.6.3 (Zhang et al., 2018) to

calculate a species tree from all gene trees, using quartet frequencies as a measure of local support (Sayyari and Mirarab, 2016).

For each gene tree, we estimated the genealogical sorting index (GSI) (Cummings et al., 2008) for (1) each of the seven populations, and (2) each of the two main lineages (i.e., north and south shaded blue and red, respectively, in Fig. 1). The GSI statistic uses rooted gene trees to quantify lineage sorting; the GSI quantifies exclusive ancestry of individuals in labelled groups by dividing the minimum number of nodes to produce monophyly for a defined group divided by the observed number of nodes necessary to connect all individuals of a group in a phylogeny. The maximum GSI value is one and occurs when a defined group is monophyletic. We calculated the GSI statistic for each sampled population and for each of the two main lineages (Fig. 1). We expect that each sampled population will show evidence of phylogenetic clustering, regardless of position in the genome. As such, GSI at the population level may have little variation tied to genomic architecture. In contrast, which populations group with which other populations are likely to be influenced by rates of lineage sorting and are therefore likely influenced by genomic architecture. As such, we may expect GSI measures at the lineage level (i.e., two main clades) to be impacted by genomic architecture.

To obtain a relative rate of molecular evolution for each population per genomic window, we calculated root-to-tip distances (RTD) in our phylogenies. For each individual across every gene tree, we calculated the RTD using the R package ape (Paradis et al., 2004). As a summary of these RTDs, we calculated the mean RTD per population relative to the maximum RTD value for each gene tree (i.e., this relative statistic's range = 0 – 1). We then measured the relationships between harmonic mean effective population sizes (mean per population) and relative RTD in regions with low recombination and high recombination, as well as the shift in values between high and low recombination regions. We also estimated relationships between these characteristics while accounting for the evolutionary relationships of the samples using

206 phylogenetic independent contrasts (PICs) calculated in the R package ape (Paradis et al.,
207 2004).
208
209 ***Genetic structure.*** We estimated genetic structure using the program ADMIXTURE v1.3.0
210 (Alexander et al., 2009). Here, we used genome-wide SNPs thinned to either a minimum of 50
211 kbp or 100 kbp distance between SNPs (datasets A and B in Table 1). We ran ADMIXTURE
212 with an assumed number of genetic clusters equal to two or seven (i.e., k = 2 and k = 7) based
213 on our knowledge of phylogeographic structure in this species from previous studies (Manthey
214 et al., 2011a, b; Manthey et al., 2015). To assess how genetic structure estimation varied across
215 the genome, we also ran ADMIXTURE for SNP datasets in non-overlapping sliding windows of
216 50 kbp and 100 kbp (datasets E and F in Table 1). We compared the genome-wide
217 ADMIXTURE results to those in each window by summing the differences in group membership
218 for each individual. In other words, this deviation value ranges from zero to nearly one, where a
219 value of zero is identical group assignment for all individuals with the same admixture
220 coefficients for each genetic cluster, and higher values indicate more dissimilar matrices.
221 We also estimated variation in genetic structure across the genome using LOSTRUCT
222 (Li and Ralph, 2019). This method runs in three steps: (1) reducing the dimensionality of the
223 data using principal component analysis (PCA) for each genomic window, (2) find distances
224 between PCA maps, and (3) using multidimensional scaling (MDS) to display variation in PCA-
225 based genetic structure across the genome. We used LOSTRUCT in sliding windows of 50 kbp
226 and 100 kbp (datasets E and F in Table 1). We used variation in MDS axis one (hereafter
227 MDS1) to describe variation in these PCA-based estimates of genetic structure across the
228 genome.
229 We expect that genomic regions with low recombination will exhibit strong
230 phylogeographic structure similar to genome-wide patterns (e.g., Fig. 1). In contrast, we expect
231 that genomic regions with high recombination will either exhibit little genetic structure or

alternative patterns of genetic structure. As such, we expect that variation in ADMIXTURE and PCA results will covary with genomic architecture.

Genetic diversity. Across 50 kbp and 100 kbp sliding windows (datasets C and D in Table 1), we measured observed heterozygosity per individual as a measure of genetic diversity.

Population genomic correlations. We used the R package Hmisc (Harrell and Dupont, 2020) to estimate both Pearson and Spearman correlation coefficients between population genomic summary statistics and characteristics of genomic architecture in sliding windows. We used the R package corrplot (Wei et al., 2017) to visualize correlations between all summary statistics. Lastly, we used variance partitioning, implemented in the R package vegan (Oksanen et al., 2007), to assess the proportion of variance in phylogeographic structure estimates explained by genomic architecture.

Population demographic history. We used the program MSMC2 v1.1.0 (Schiffels and Durbin, 2014) to estimate demographic history for each individual. For use in MSMC, we masked regions of the genome not genotyped due to low coverage or low genotype quality scores. Additionally, we did not include the sex chromosomes in demography calculations. We ran MSMC for each individual allowing up to 20 iterations (default setting) and used up to 23 inferred distinct time segments because this setting worked well to reduce spurious or inconsistent results in other songbirds that we have studied (Manthey et al., 2022). We performed 10 bootstraps for each demography estimate, using 1 Mbp bootstrapped segments of the genome, to assess how demographic signal varies when subsetting parts of the genome. Because the output of MSMC is interpreted relative to assumed mutation rates and generation times, we used the Brown Creeper genome mutation rate estimate of 2.506×10^{-9} substitutions per site per year (Manthey et al., 2021). Because there are no published estimates of Brown

Creeper generation times, we used a proxy generation time of double the age of sexual maturity (Nadachowska-Brzyska et al., 2015) using maturity estimates from the Animal Aging and Longevity Database (age of maturity = one year) (Tacutu et al., 2017). With the MSMC demographic model output, we estimated the harmonic mean population sizes for each population by using the mean MSMC population size estimates for each individual in 1000-year discrete time intervals over the past 200 kya.

Code availability. All computer code used for analyses and figure creation (applicable for some figures) for this project is available here: github.com/jdmanthey/certhia_phylogeography. We used the following R packages for figure creation and file manipulation that were not cited in other parts of the methods section: Biostrings (Pagès et al., 2017), ggplot2 (Wickham, 2011), palettetown (Lucas, 2016), phytools (Revell, 2012), and RcolorBrewer (Neuwirth, 2014).

RESULTS

Genome-wide phylogeographic structure and demography. We used genomic sequencing data from 21 ingroup individuals sequenced at ~18-29× genomic coverage to estimate genome-wide patterns of phylogeographic structure. We corroborated previous genetic work (that used few to thousands of genetic markers) by identifying hierarchical and strong phylogeographic structure among sampled populations (Manthey et al., 2011a, b; Manthey et al., 2015). The deepest phylogenomic split separates northern from southern populations and there is additional support for distinctiveness of each of the regionally sampled populations (Fig. 1C). Genome-wide ADMIXTURE results were consistent across different thinning strategies (i.e., 50 kbp and 100 kbp thinning; only 50 kbp results plotted) and showed patterns of genetic structure that aligned well with the species tree (Fig. 1C). Demographic history estimates for each individual were consistent within populations, but each population exhibited a distinct

demographic history (Fig. 1D). In the Pacific and Central American localities, population sizes have fluctuated somewhat, but generally stay below an N_E of 200,000 over the past 100 ky (Fig. 1D). The Sierra Madre Oriental population showed evidence for a sharp decline in N_E over the past 50 ky, shifting from an N_E ~ 200,000 at about 50 kya to an N_E ~ 10,000 in the past ten kya (Fig. 1D). The Rocky Mountains population has remained relatively stable over the past 100 ky with an N_E ~ 200,000 (Fig. 1D). Lastly, the Eastern North America and Central Mexico populations have exhibited fluctuations and much larger N_E than all other populations over the past 100 ky (Fig. 1D). Harmonic mean effective population sizes over the past 200 ky ranged from ~85,000 (Central America South) to ~320,000 (Central Mexico) (Fig. 1D). Harmonic mean effective population size estimates over the past 200 ky are highly correlated with observed heterozygosity estimates for each individual (r = 0.962).

Genetic diversity. Genetic diversity in each individual varied widely across the genome, with mean observed heterozygosity values for each individual between ~0.00165 and 0.00463 (Fig 1B). Observed heterozygosity was strongly correlated across the genome in all pairwise comparisons of individuals (mean r = 0.409, range = 0.189 – 0.853; all $p << 0.001$). Notably, the Sierra Madre Oriental, Pacific, and Central American localities had more windows with no heterozygosity than the other populations (Fig. 1B).

Phylogeographic structure variation across the genome. We estimated phylogeographic structure across the genome using PCA, ADMIXTURE, and the GSI metric from phylogenies; all estimates of phylogeographic structure varied across the genome, with the outliers deviating the most from genome-wide patterns clustering mostly on small chromosomes and the ends of large chromosomes (Fig. 2; Fig. S2). The most extreme deviations from genome-wide phylogeographic structure appear to cluster the Central Mexico population with the northern lineage (Fig. S3), and in some cases also cluster the Sierra Madre Oriental population with the

northern lineage (Fig. S3; Fig. 3). As an example, we plot the phylogeographic structure for one of these outlier windows in Fig. 3, demonstrating the clustering of the Sierra Madre Oriental and Central Mexico populations with the northern lineage.

Correlations between phylogeographic structure estimates and genomic architecture. We found a strong correlation between different measures of phylogeographic structure, including GSI at the lineage level, MDS1 of the PCA, and ADMIXTURE deviations (all $r \geq 0.58$; $p <<< 0.001$; Fig. 4; Fig. S4). In contrast, GSI at the population level did not vary consistently with the other metrics (all r between -0.21 and -0.03), likely because the population-level GSI usually showed similar patterns across the genome (i.e., individuals generally clustered with individuals sampled from the same population).

Phylogeographic structure patterns most different from genome-wide patterns were strongly positively correlated with recombination rate, GC content, and genetic diversity (Fig. 4; Fig. S4). In contrast, TE content had no or weak correlations with all other statistics that we calculated (Fig. 4; Fig. S4). Correlations were consistent between 50 kbp and 100 kbp estimates, with no correlations deviating more than ~0.08 when estimated with different window sizes (Fig. S4).

Using variance partitioning, recombination rate variation most strongly explained deviations in phylogeographic structure, but interactions of recombination rate, GC content, CDS content, and TE content also explained some portions of the variance (Table 2). Most notably, genomic architecture explained approximately 60% of the variance in both (1) the MDS1 axis explaining differences in PCA-based estimates of phylogeographic structure and (2) ADMIXTURE results at the lineage level with an assumed k = 2 (Table 2).

The relationship between recombination rate and phylogeographic structure is exemplified when comparing the genomic windows with the highest or lowest values of recombination rate; estimates of phylogeographic structure and genetic diversity have little to no

336 overlap in statistic distributions in high recombination regions versus low recombination regions
337 (Fig. 5). These patterns hold regardless of whether we are looking at autosomes or the Z
338 chromosome (Fig. 5).

339 Because the effective population sizes for each locality varied substantially (Fig. 1; Fig.
340 S5), we looked to see if there was a relationship between relative RTD and population size in
341 regions with very different recombination rates. Using both the raw measurements and PICs, we
342 found a negative association between relative rates of molecular evolution and harmonic mean
343 effective population sizes (Fig. 6; Fig. S6). Notably, there was also a strong positive association
344 between effective population sizes and shifts in relative rates of molecular evolution between
345 high and low recombination regions (Fig. 6).

346

347 **DISCUSSION**

348

349 Using whole-genome sequencing for seven populations of the Brown Creeper, we aimed to
350 decipher how genome architecture influences phylogeographic structure variation across the
351 genome. We found that recombination rate and other characteristics of the genome explain 6-
352 68% of the variance in phylogeographic structure inference using different metrics and genomic
353 sliding window sizes (Table 2).

354

355 ***Phylogeographic structure shaped by genomic architecture.***

356

357 We used genetic clustering, ordination, and phylogenetic methods to assess phylogeographic
358 structure in genomic sliding windows. We found that recombination rate variation was the
359 strongest predictor of phylogeographic structure variation across the genome (Table 2).
360 Consistent with our expectation, phylogeographic signal best representing the bifurcating
361 evolutionary history of the Brown Creeper was identified in genomic regions with relatively low

recombination rate; this was consistent across all methods used (Fig. 2). Notably, the genomic windows with the lowest recombination rates deviated little from the genome-wide patterns (Fig. 5).

Previous work in insects, birds, and mammals has shown that phylogenomic signal varies across the genome (Edelman et al., 2019; Fontaine et al., 2015; Li et al., 2019; Martin et al., 2019; Thom et al., 2024). Generally, these studies have found or suggested that the background species tree is best represented by phylogenomic patterns exhibited in genomic regions with low recombination, and that gene flow among taxa is more prevalent in genomic regions with high recombination rate (Edelman et al., 2019; Li et al., 2019; Martin et al., 2019; Thom et al., 2024). Our results in the Brown Creeper echo these findings *at a shallow evolutionary timescale*, whereby we find highest support for the genome-wide supported phylogeographic relationships in genomic regions with low recombination rate (Fig. 2; Fig. S2). We may interpret these patterns in the context of lineage sorting during the speciation process, whereby genomic regions with low introgression exhibit quicker polymorphism fixation due to relatively increased effects of linked selection and genetic drift and reduced homogenization among lineages due to gene flow.

Genomic studies investigating intraspecific population and phylogeographic structure have more commonly used PCA-based methods (e.g., LOSTRUCT) to investigate variation in genomic structure across the genome. In two species of woodpeckers, a small portion of the variance in PCA-based phylogeographic structure was found to be associated with local recombination rate (Moreira et al., 2023). We found that variation in phylogeographic structure across the genome of the Brown Creeper—inferred using both ordination and genetic clustering methods—was strongly associated with recombination rate variation (Fig. 2; Fig. S2; Table 2). We may infer that the same interactions between recombination rate variation and population genomics processes shaping variance in phylogenomic signal are also shaping variance in clustering- and ordination-based estimates of phylogeographic structure.

In contrast to generalizations about low recombination regions often reflecting a taxon's background evolutionary history, in some scenarios we may expect regions of extremely low recombination to greatly differ from genome-wide signatures of population genetic structure. In several taxa, including sunflowers, flies, fishes, and birds, the greatest deviations from the genome-wide pattern of intraspecific population structure (inferred with PCA) have been identified in genomic regions with extremely low recombination rates that are often inferred to be polymorphic inversions within populations or species (Hale et al., 2021; Huang et al., 2020; Li and Ralph, 2019; Mérot et al., 2021; Perrier et al., 2020; Shi et al., 2021; Todesco et al., 2020; Whiting et al., 2021). In these cases, if a taxon has relatively little population structure but also exhibits polymorphic inversions, we may expect the biggest deviations in population genetic structure from genome-wide patterns to reflect these polymorphic inversions that exhibit suppressed recombination. These cases present interesting patterns to think about when interpreting genomic phylogeography data. Genomic regions with low recombination may best represent a taxon's evolutionary history, excepting times when these regions are associated with large structural variants.

Interaction of recombination rate, population demography, and rate of evolution.

While we may expect that the interactions between recombination rate and population genomics processes will impact the rate of evolution across the genome, we did not simply observe little phylogeographic structure in genomic regions with high recombination rates and strong phylogeographic structure in genomic regions with low recombination rates. Conversely, we found strong—and differing—patterns of phylogeographic structure across the genome (Fig. 1; Fig. 3; Fig. S3). Because these differing patterns of phylogeographic structure generally separated the Central American populations and sometimes the Sierra Madre Oriental

population from all others, we hypothesized that populations with relatively smaller N_E exhibit relatively higher evolutionary rates in genomic regions with high recombination.

Using relative RTD measures as a relative rate of molecular evolution for each population, we found that larger populations exhibited reduced rates of molecular evolution in genomic windows with high recombination rates (Fig. 6; Fig. S6) and that shifts in relative rates of molecular evolution in high versus low recombination genomic regions were positively associated with effective population sizes (Fig. 6; Fig. S6). This is consistent with simulations by Tigano and colleagues (2021) where the authors showed the interplay between recombination rate and selection causes greater genomic variance in evolutionary rates in larger populations relative to more consistent evolutionary rates across the genome in smaller populations.

We suspect that molecular evolution in genomic regions with high recombination rates is a product of complex interactions between population demography and the relative strengths of linked selection and genetic drift. In the Brown Creeper genome, recombination rate variation is positively associated with gene density (Fig. 2; Fig. 4) and we may interpret gene-dense genomic regions as targets for natural selection. Indeed, in a previous study in the Brown Creeper (Manthey et al., 2021), we showed that the two main Brown Creeper lineages exhibited relatively less neutral evolution in the gene-dense microchromosomes relative to the larger macrochromosomes. In gene-dense and high recombination regions under the effects of purifying selection, we may expect populations with relatively smaller N_E to accumulate substitutions faster than populations with higher N_E (Lanfear et al., 2014), consistent with the trends we identified here in the Brown Creeper (Fig. 6; Fig. S6).

Implications for future phylogeographic studies

If phylogeographic structure varies widely across the genome, what are realistic and best-practice approaches for future phylogeographic work? Are studies that use few genes or

reduced representation genomic datasets doomed to be wrong from the start? We expect that strong phylogeographic structure will be detected even with few genetic markers. For example, more than ten years ago we used 20 genetic markers obtained with Sanger sequencing to study the phylogeography of the Brown Creeper (Manthey et al., 2011b) and found the same general phylogeographic trends observed here with our whole-genome dataset. In contrast, any study where most of the genetic markers are taken from genomic regions where the pattern differs from a taxon's true evolutionary history (e.g., high recombination regions in the Brown Creeper case) may run into problems inferring that true history. Additionally, in any taxa with weak population genetic structure or widespread and rampant gene flow, a whole-genome method may be the only approach to identify the few genomic regions differentiating taxa (e.g., Toews et al., 2016). Overall, we suggest using the most amount of genetic data feasible for future phylogeographic studies given sources of biological material (e.g., quality of preserved tissue) and funding available, as well as investigating the patterns and potential causes of population genetic structure variation across the genome when possible.

CONCLUSIONS

We used whole genome sequencing to estimate how genomic architecture shapes variation in phylogeographic structure across the genome of the Brown Creeper. We found that phylogeographic structure—as measured using ordination, phylogenetic, and clustering methods—was strongly associated with regional genomic variation in recombination rates. In low recombination regions, we recovered phylogeographic structure concordant with genome-wide patterns with all three types of methods. The most divergent phylogeographic patterns were in high recombination regions; populations with small effective population sizes were distinct from all other populations due to relatively faster evolution than larger populations in these high recombination regions. Because these high recombination regions are rich in coding

genes, we hypothesize that large populations have higher relative effects of purifying selection in these regions, and overall slower relative molecular evolutionary rates compared to smaller populations. Overall, our results show that phylogeographic structure may vary widely across the genome, and that effective population sizes of sampled populations and genomic architecture and their interactions will impact regional genomic variation in phylogeographic structure.

ACKNOWLEDGEMENTS

We would like to thank the collection managers, curators, and contributors for generous tissue loans for all individuals used in this study from the following museums: Burke Museum of Natural History and Culture, and University of Kansas Biodiversity Institute. Sequencing was supported by Texas Tech University start-up funding to JDM and a generous donation from the Ferguson family to GMS and the Denver Museum of Nature and Science. Support was also provided by NSF awards #1953688 to JDM and #0814841 to GMS. The High-Performance Computing Center at TTU supported computational analyses.

DATA ACCESSIBILITY

All raw resequencing data uploaded to NCBI's SRA database under BioProject PRJNA1068991. All code used for analysis on this project is available on GitHub: (github.com/jdmanthey/certhia_phylogeography).

AUTHOR CONTRIBUTIONS

JDM and GMS designed the study. JDM performed laboratory and bioinformatic work and wrote the first draft of the manuscript. JDM and GMS contributed to revising and improving the final draft of the manuscript.

DECLARATION OF INTEREST

The authors declare no conflicts of interest.

TABLES AND FIGURES

Figure 1. Sampling map, genetic diversity, phylogeographic structure, and demography. (A) Sampling localities for this study. Colors for localities are consistent across plots. (B) Violin plots of observed heterozygosity across all 50 kbp sliding windows. White circles indicate means. (C) Consensus phylogeny using 19,639 gene trees from the 50 kbp windows. Support values are labelled for all branches showing the highest support from all estimation methods (N = 4), including consensus and ASTRAL phylogenies for both the 50 kbp and 100 kbp window datasets. At tips of phylogeny are ADMIXTURE results from 19,602 genome-wide SNPs (thinned every 50 kbp) for either two or seven assumed genetic clusters (k = 2 or k = 7, respectively). (D) Demographic history estimated with MSMC2. Different individuals are represented with differently colored lines and bootstraps are shown with thin lines. In (D), HM = harmonic mean. Brown Creeper photo in (A) by JDM from the Chiricahua Mountains in southern Arizona.

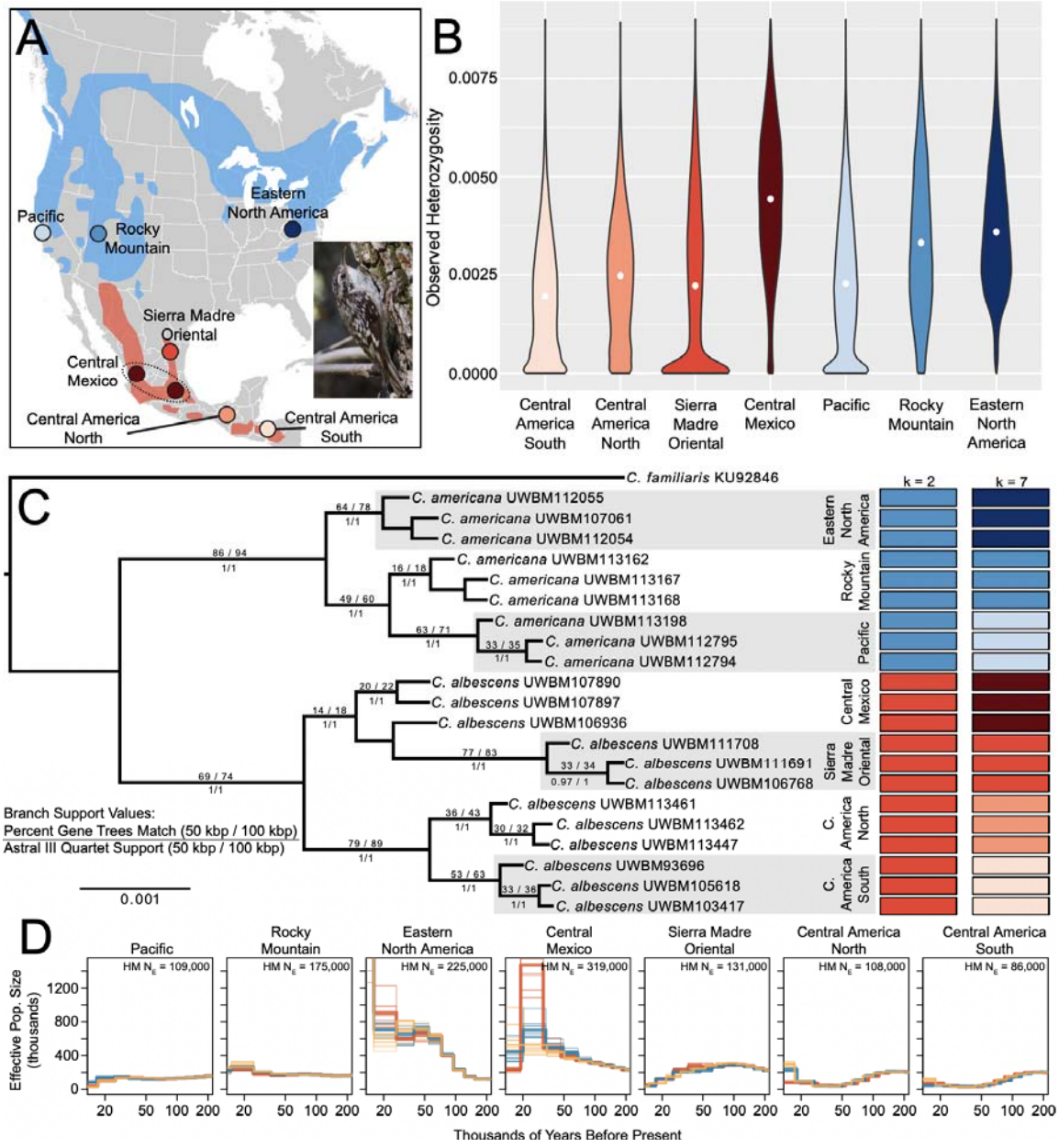

Figure 2. Genomic architecture and phylogeographic structure variation across the genome in 50kbp sliding windows. Gray points indicate window values and dark gray lines indicate means across 20 windows (i.e., 1 Mbp windows). Blue indicates top 2.5% of outliers and orange indicates bottom 2.5% of outliers for each statistic. Bottom outliers not shown for CDS, ADMIX., and GSI as these each have large proportions of values equal to zero. Abbreviations: mean effective recombination rate of the two main lineages (ρ), gene content (CDS), transposable element and repetitive DNA content (TE), multidimensional scaling axis one from principal components analyses (-MDS1), mean genealogical sorting index for the two main *Certhia* lineages (1 - GSI), ADMIXTURE deviation relative to genome-wide analysis (ADMIX.), and mean genetic diversity across individuals as measured using observed heterozygosity (H_O). MDS1 is plotted as negative and GSI is plotted as (1 - GSI) so that deviations from expected phylogeographic structure for MDS1, GSI, and ADMIXTURE are all represented as higher values.

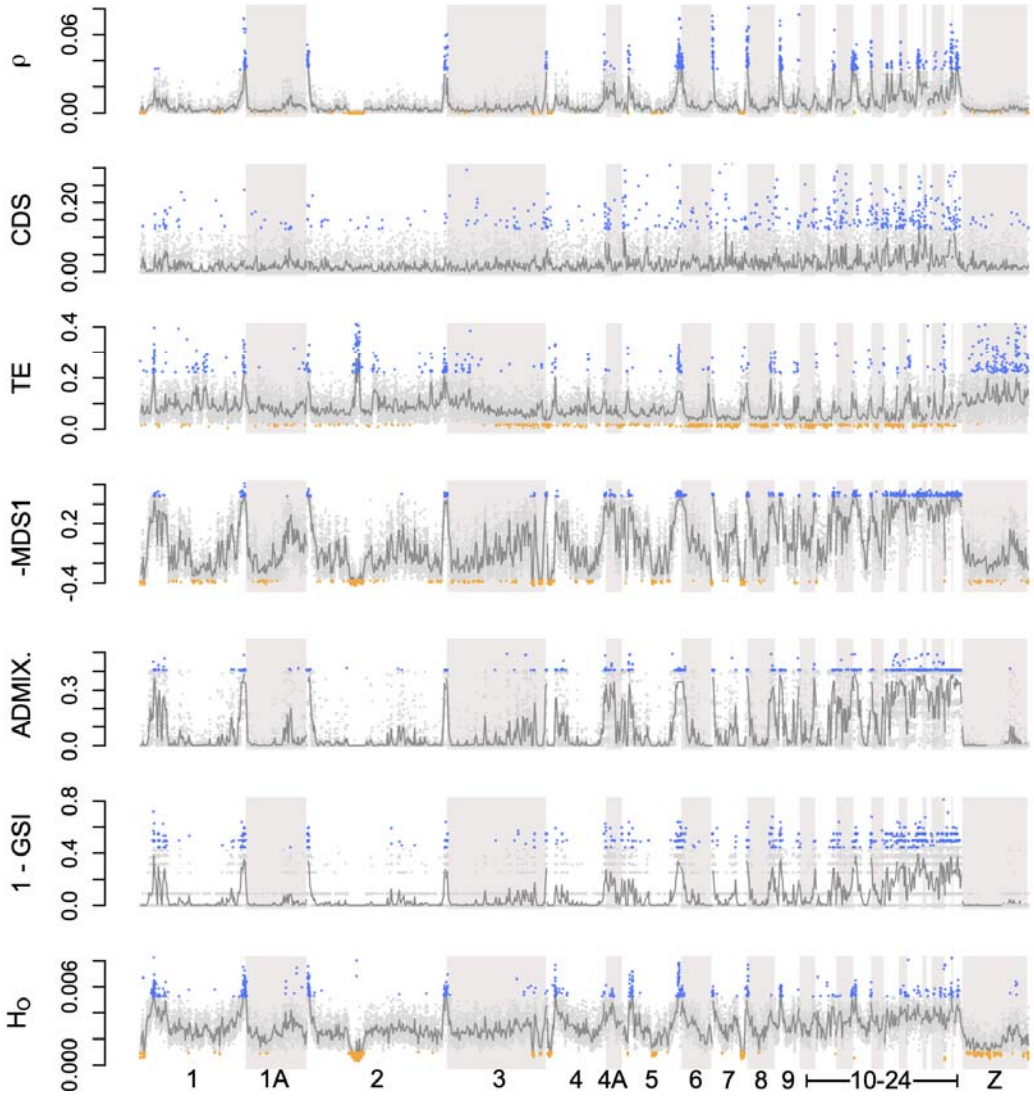

548 Figure 3. Example phylogeographic structure in a window that deviates from genome-wide
549 patterns. This window had the 15th lowest MDS1 value of all windows from the principal
550 components analysis (PCA) across the genome. (A) PCA, (B) RAxML phylogeny, and (C)
551 ADMIXTURE results for a window on chromosome 4.

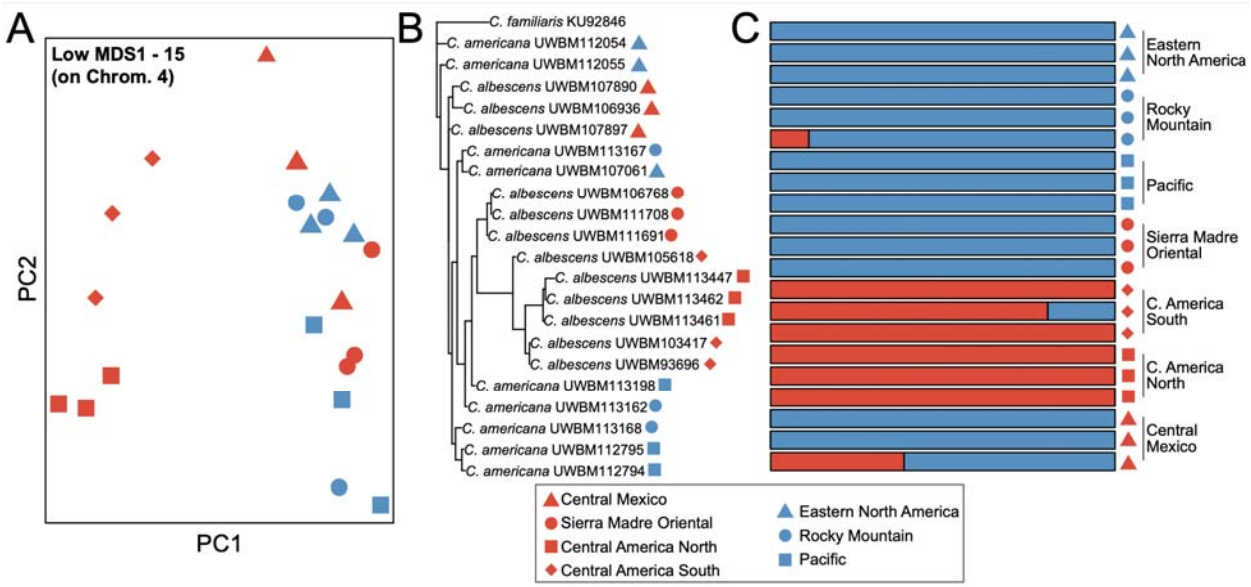

552
553
554
555
556
557
558
559
560
561
562
563
564
565
566
567
568
569
570
571

Figure 4. Correlation plot of genomic architecture, genomic diversity, and phylogeographic structure for 50 kbp windowed statistics. Pearson's and Spearman's r coefficients are plotted above and below the diagonal, respectively. Abbreviations shown in plot: mean effective recombination rate of the two main lineages (ρ); GC content (GC%); gene content (CDS%); transposable element content (TE%); mean observed heterozygosity (H_O); genealogical sorting index at the population [1 - GSI (Pop.)] and lineage [1 - GSI (Lin.)] levels; negative multidimensional scaling axis one from principal components analyses (-MDS1); ADMIXTURE deviation relative to genome-wide analysis for two [ADMIX. (k = 2)] or seven [ADMIX. (k = 7)] assumed genetic clusters.

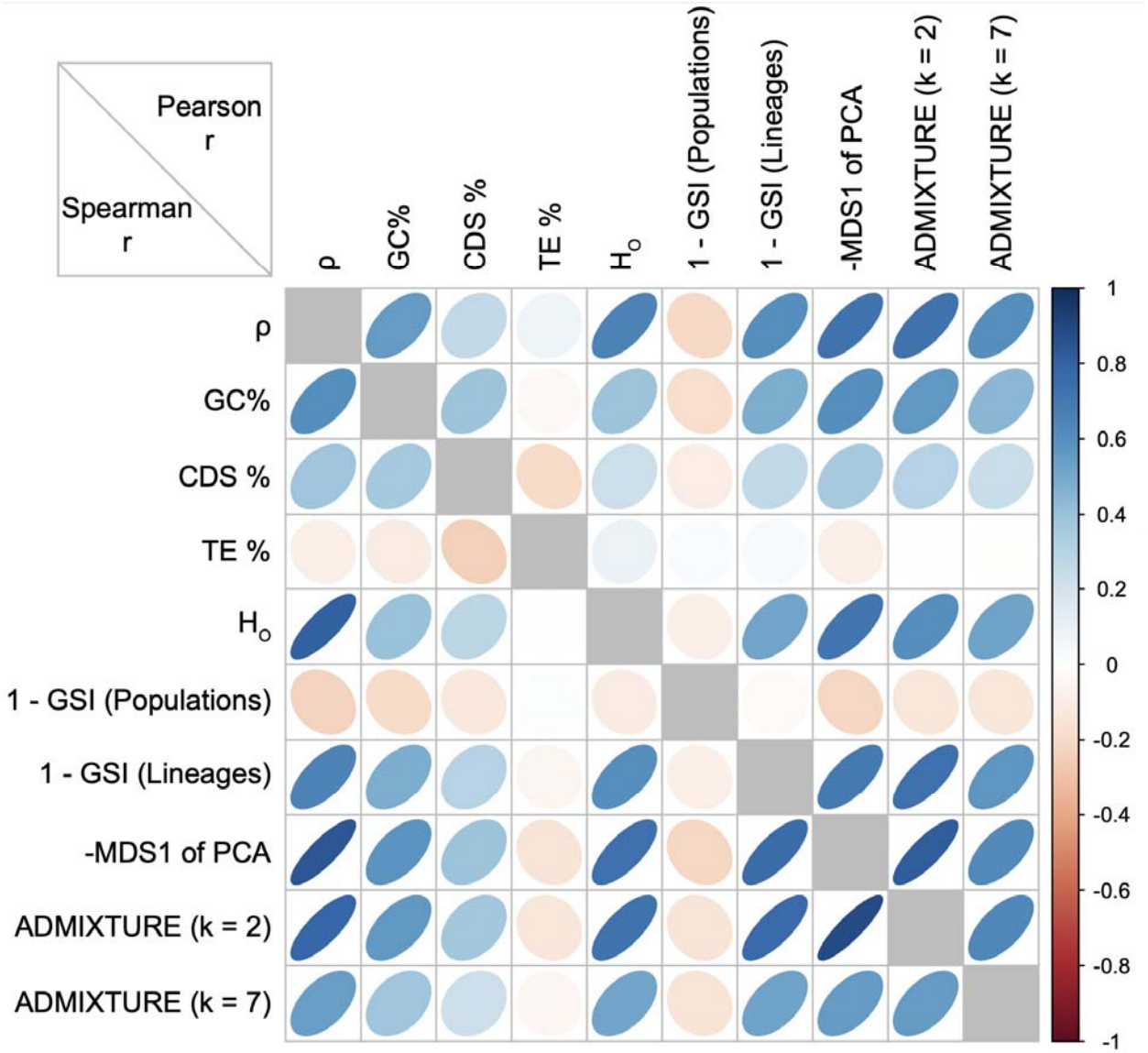

Figure 5. Violin plots of phylogeographic structure variation in genomic regions with very high or low recombination rates, separated for autosomal (A) and Z-linked (Z) genomic regions. 50 kbp windows with the highest or lowest 2.5% of recombination rate values are included. Higher values for ADMIXTURE deviations, 1 - GSI, and -MDS1 indicate values deviating relatively more from the genome-wide patterns of phylogeographic structure.

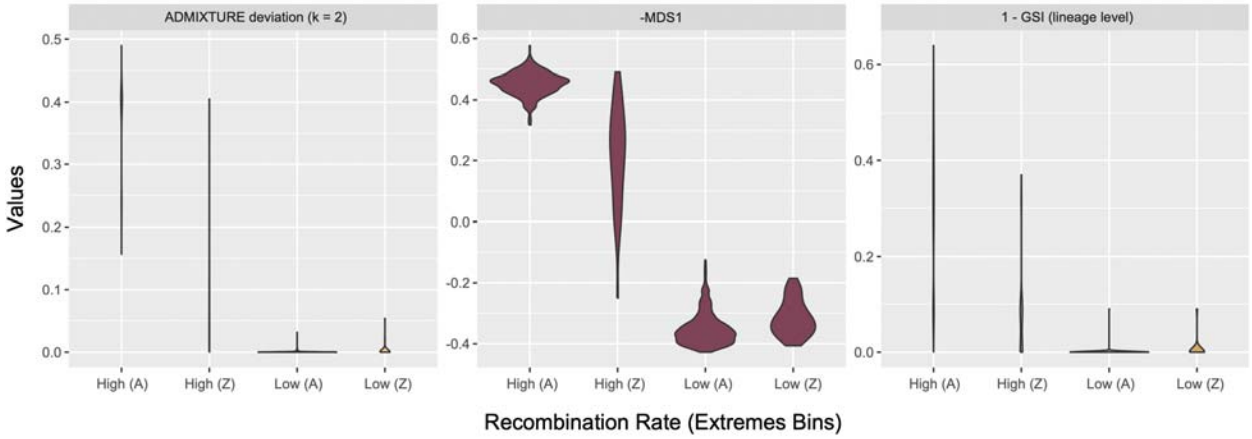

Figure 6. Relationship between effective population sizes and rate of evolution (measured by relative root-to-tip distance for each population) in genomic regions that vary in recombination rate. Extreme low and high recombination (rho) regions represent the quintiles of the genome with the lowest or highest recombination rates (i.e., highest 20% and lowest 20% of windows). Results for raw data are shown in (A-C) and for phylogenetic independent contrasts (PIC) in (D-F). The right panels in each row (C + F) show the shift in relative rates of evolution between high and low recombination genomic regions.

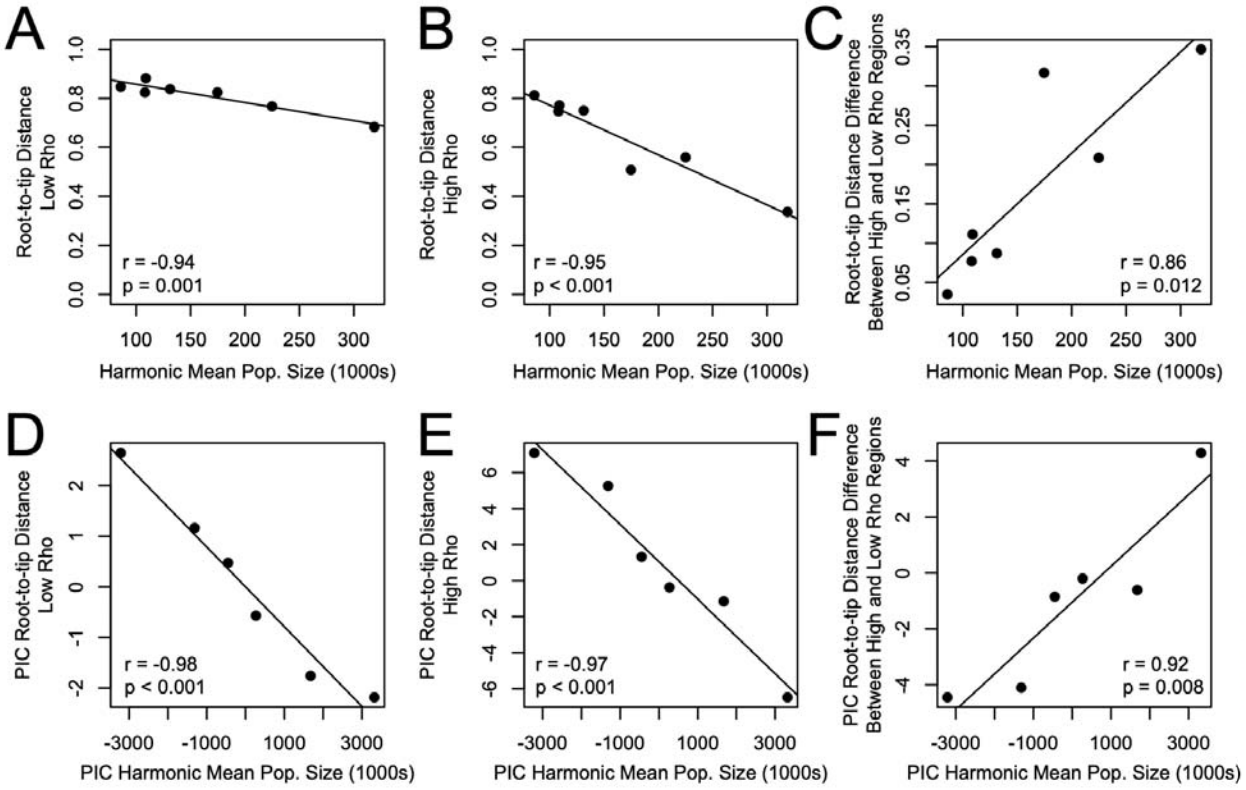

Table 1. Different datasets used in this study and their characteristics. For inclusion, all datasets required sites to have a minimum quality score of 20, minimum of 20 genotype quality, a minimum depth per individual for a site to be called of 6, and a max mean depth across individuals of 50.

Set	Missing Allowed	OG[1]	Window size	# Windows	Min. Sep. per SNP[2]	# SNPs	# Sites	Analyses
A	0%		-	-	50 kbp	19,602	19,602	Genome-wide ADMIXTURE
B	0%		-	-	100 kbp	9,838	9,838	Genome-wide ADMIXTURE
C	20%	X	50 kbp	19,713	-	35,463,408	890,335,872	RAxML, GSI, H_O
D	20%	X	100 kbp	9,862	-	35,463,408	890,335,872	RaxML, GSI, H_O
E	0%		-	-	-	21,657,220	21,657,220	LOSTRUCT
F	0%		50 kbp	19,697	-	21,657,220	21,657,220	ADMIXTURE per window
G	0%		100 kbp	9,860	-	21,657,220	21,657,220	ADMIXTURE per window
H	0%		-	-	-	*	*	MSMC2

[1]OG = outgroup included

[2]Min. Sep. per SNP = minimum separation between SNPs (i.e., thinning)

*SNPs and sites not labeled for MSMC2 analyses because these values varied per individual. For each individual, no missing data was allowed for that particular individual's MSMC2 demographic analyses input files. The MSMC2 dataset did not include the Z chromosome.

Table 2. Variance partitioning where the explanatory variables are characteristics of genomic architecture and response variables are different measures of population genetic structure. Values indicative of variance proportion explained by each explanatory variable or their interactions.

50 kbp windows						
Measure of Genetic Structure	ρ	CDS	TE	GC	Interactions	Total
MDS1	0.23	0.00	0.01	0.04	0.33	0.61
GSI (Lineages)	0.16	0.00	0.00	0.02	0.22	0.40
GSI (Populations)	0.02	0.00	0.00	0.01	0.03	0.06
ADMIXTURE (k = 2)	0.24	0.00	0.00	0.03	0.30	0.57
ADMIXTURE (k = 7)	0.19	0.00	0.00	0.01	0.18	0.38
100 kbp windows						
Measure of Genetic Structure	ρ	CDS	TE	GC	Interactions	Total
MDS1	0.22	0.01	0.01	0.03	0.41	0.68
GSI (Lineages)	0.16	0.00	0.00	0.01	0.23	0.40
GSI (Populations)	0.02	0.00	0.00	0.01	0.05	0.08
ADMIXTURE (k = 2)	0.25	0.00	0.00	0.02	0.35	0.62
ADMIXTURE (k = 7)	0.20	0.00	0.00	0.01	0.22	0.43

SUPPLEMENTAL TABLES AND FIGURES

Table S1. Sampling metadata and characteristics of sequencing amount and coverage when aligned to the reference genome. Samples from Utah, Morelos, Jalisco, and the outgroup were retrieved from the NCBI SRA and originally sequenced for a previous study by Manthey and colleagues (2021).

Museum #	Lineage	Locality	Lat.	Long.	Raw bp	Filtered bp	Coverage
UWBM103417	South	Copan, HN	14.866	-89.050	40,501,485,458	34,714,897,849	22.79
UWBM105618	South	Copan, HN	14.866	-89.050	30,149,924,172	26,420,616,801	18.55
UWBM93696	South	Copan, HN	14.866	-89.050	40,591,948,048	36,089,400,965	26.06
UWBM113447	South	Chiapas, MX	16.691	-92.606	37,741,499,908	33,063,229,986	23.32
UWBM113461	South	Chiapas, MX	16.691	-92.606	32,696,721,580	27,488,157,228	18.51
UWBM113462	South	Chiapas, MX	16.691	-92.606	48,519,014,074	42,841,474,607	27.09
UWBM106936	South	Morelos, MX	19.0873	-99.194	40,136,994,108	35,563,542,819	26.35
UWBM107890	South	Jalisco, MX	21.882	-103.865	43,601,103,228	38,563,138,625	26.14
UWBM107897	South	Jalisco, MX	21.882	-103.865	30,536,607,690	27,038,872,945	18.55
UWBM106768	South	Nuevo Leon, MX	24.872	-100.224	42,330,853,397	37,109,282,807	27.62
UWBM111691	South	Nuevo Leon, MX	24.872	-100.224	41,523,724,956	36,804,470,356	26.21
UWBM111708	South	Nuevo Leon, MX	24.872	-100.224	43,392,483,440	36,820,385,840	27.04
UWBM113198	North	California, US	36.245	-121.700	40,117,812,880	35,379,027,102	26.26
UWBM112794	North	California, US	36.245	-121.553	37,692,762,846	33,128,089,974	23.33
UWBM112795	North	California, US	36.245	-121.553	44,376,620,806	38,809,177,747	28.71
UWBM113162	North	Utah, US	37.317	-113.455	40,934,172,636	36,217,919,293	26.25
UWBM113168	North	Utah, US	37.317	-113.455	39,295,062,200	34,925,676,137	25.72
UWBM113167	North	Utah, US	37.377	-113.467	42,535,860,138	37,425,027,332	27.55
UWBM107061	North	West Virginia, US	38.289	-79.937	43,886,484,470	38,699,509,454	28.65
UWBM112055	North	West Virginia, US	38.289	-79.937	47,972,794,224	40,458,960,409	29.36
UWBM112054	North	West Virginia, US	38.641	-79.838	39,431,412,482	34,774,499,050	25.96
KU92846	Outgroup	England			21,417,629,506	19,195,682,239	13.58

Figure S1. Sequencing coverage aligned to the reference genome for each individual. The vertical red lines indicate the mean coverage per individual.

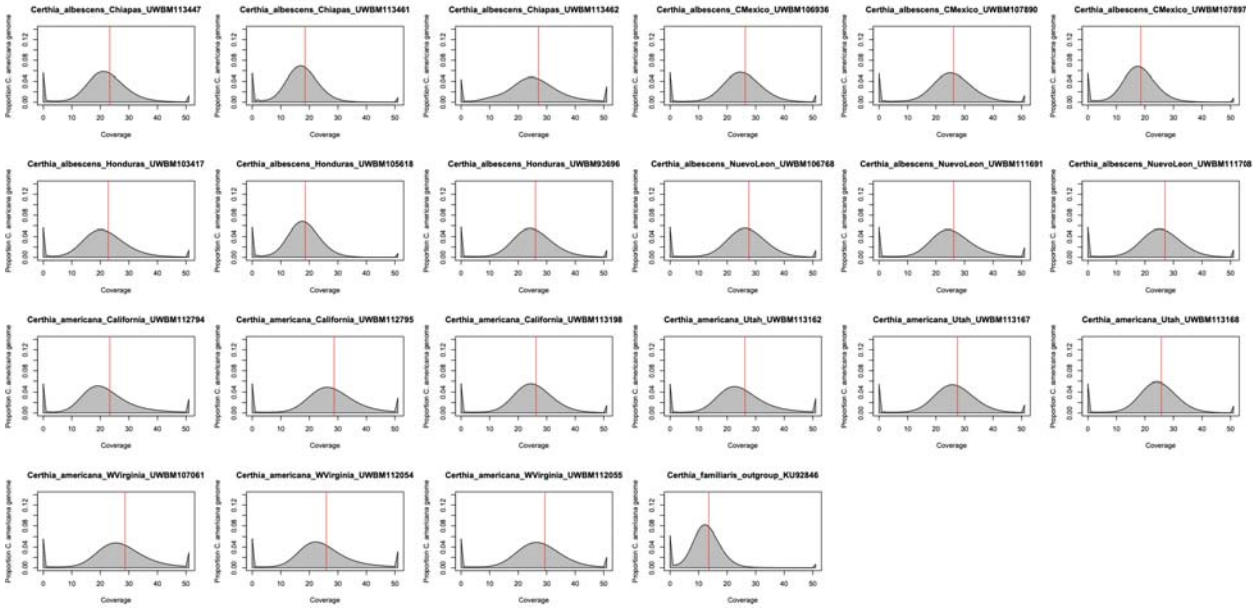

Figure S2. Genomic architecture and phylogeographic structure variation across the genome in 100kbp sliding windows. Gray points indicate window values and dark gray lines indicate means across ten windows (i.e., 1 Mbp windows). Blue indicates top 2.5% of outliers and orange indicates bottom 2.5% of outliers for each statistic. Bottom outliers not shown for CDS, ADMIX., and GSI as these each have large proportions of values equal to zero. Abbreviations: mean effective recombination rate of the two main lineages (ρ), gene content (CDS), transposable element and repetitive DNA content (TE), multidimensional scaling axis one from principal components analyses (-MDS1), mean genealogical sorting index for the two main *Certhia* lineages (1 - GSI), ADMIXTURE deviation relative to genome-wide analysis (ADMIX.), and mean genetic diversity across individuals as measured using observed heterozygosity (H_O). MDS1 is plotted as negative and GSI is plotted as (1 - GSI) so that deviations from expected phylogeographic structure for MDS1, GSI, and ADMIXTURE are all represented as higher values.

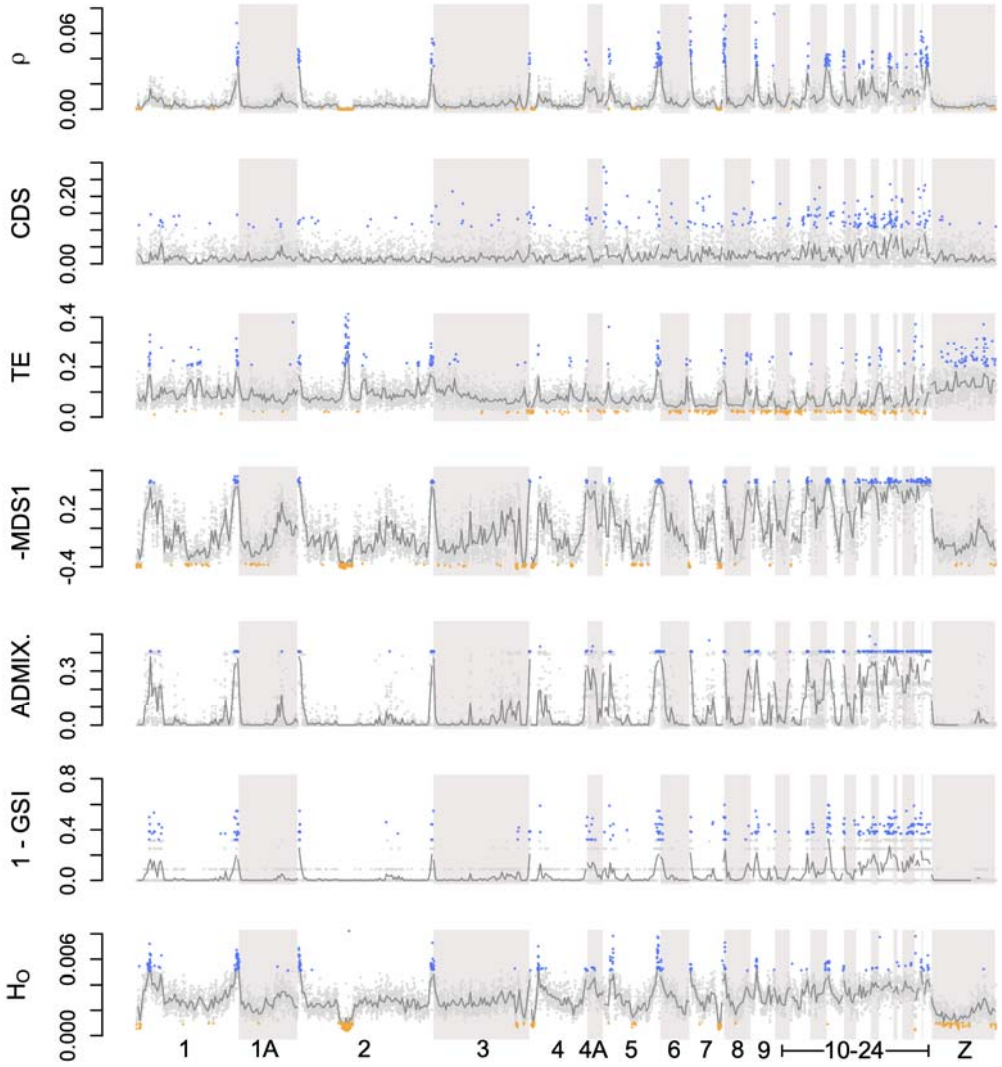

696 Figure S3. The 15 most extreme outlier principal components analysis (PCA) windows identified
697 from those windows with low MDS dimension one values.

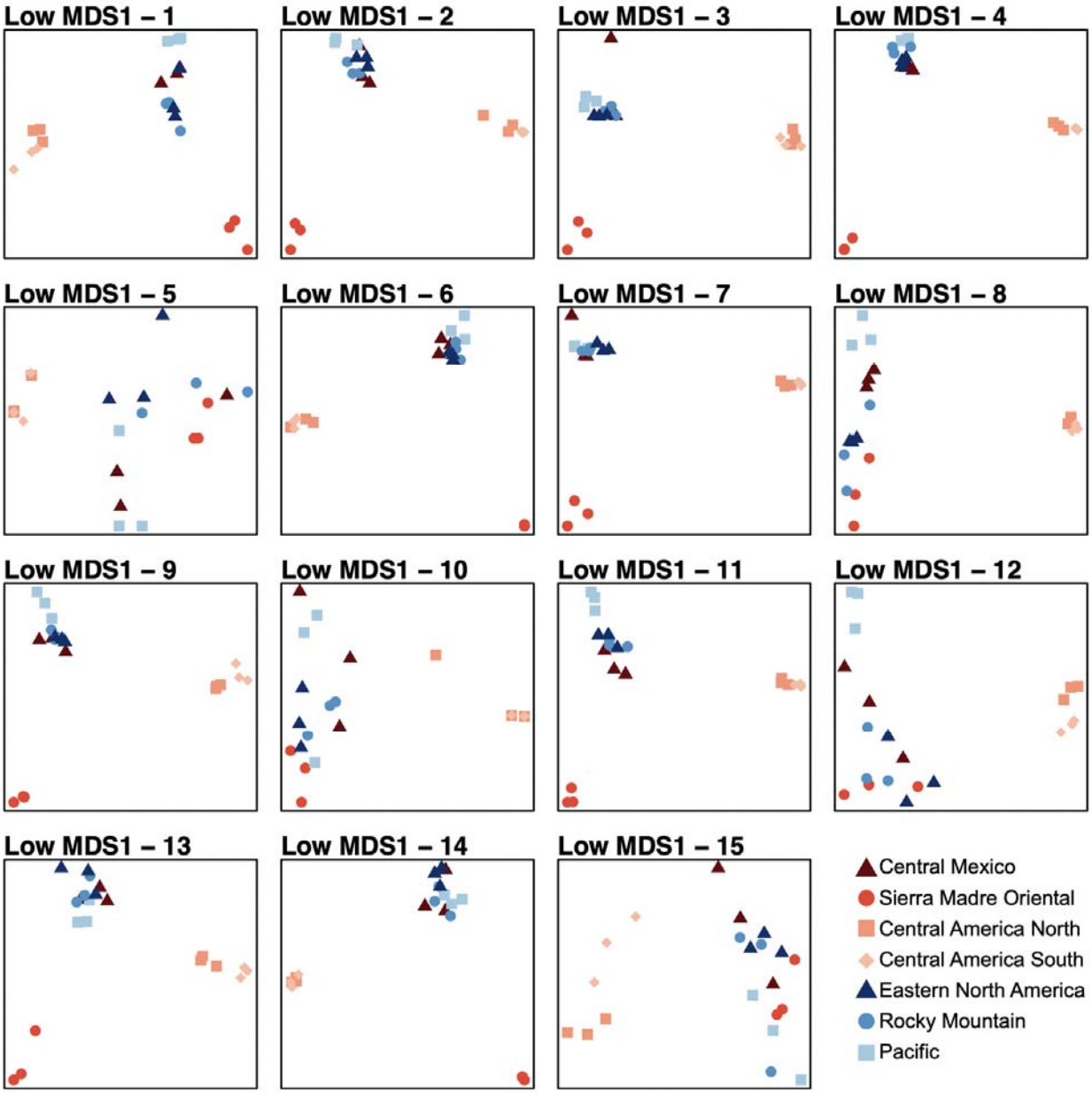

698
699
700
701
702
703
704
705

Figure S4. Correlation plot of genomic architecture, genomic diversity, and phylogeographic structure for (A) 50 kbp and (B) 100 kbp windowed statistics. Pearson's and Spearman's r coefficients are plotted above and below the diagonal, respectively. In (C), the absolute value difference between correlations in 50 kbp and 100 kbp windows. Abbreviations shown in plot: mean effective recombination rate of the two main lineages (ρ); GC content (GC%); gene content (CDS%); transposable element content (TE%); mean observed heterozygosity (H_O); genealogical sorting index at the population [1 - GSI (Pop.)] and lineage [1 - GSI (Lin.)] levels; negative multidimensional scaling axis one from principal components analyses (-MDS1); ADMIXTURE deviation relative to genome-wide analysis for two [ADMIX. (k = 2)] or seven [ADMIX. (k = 7)] assumed genetic clusters.

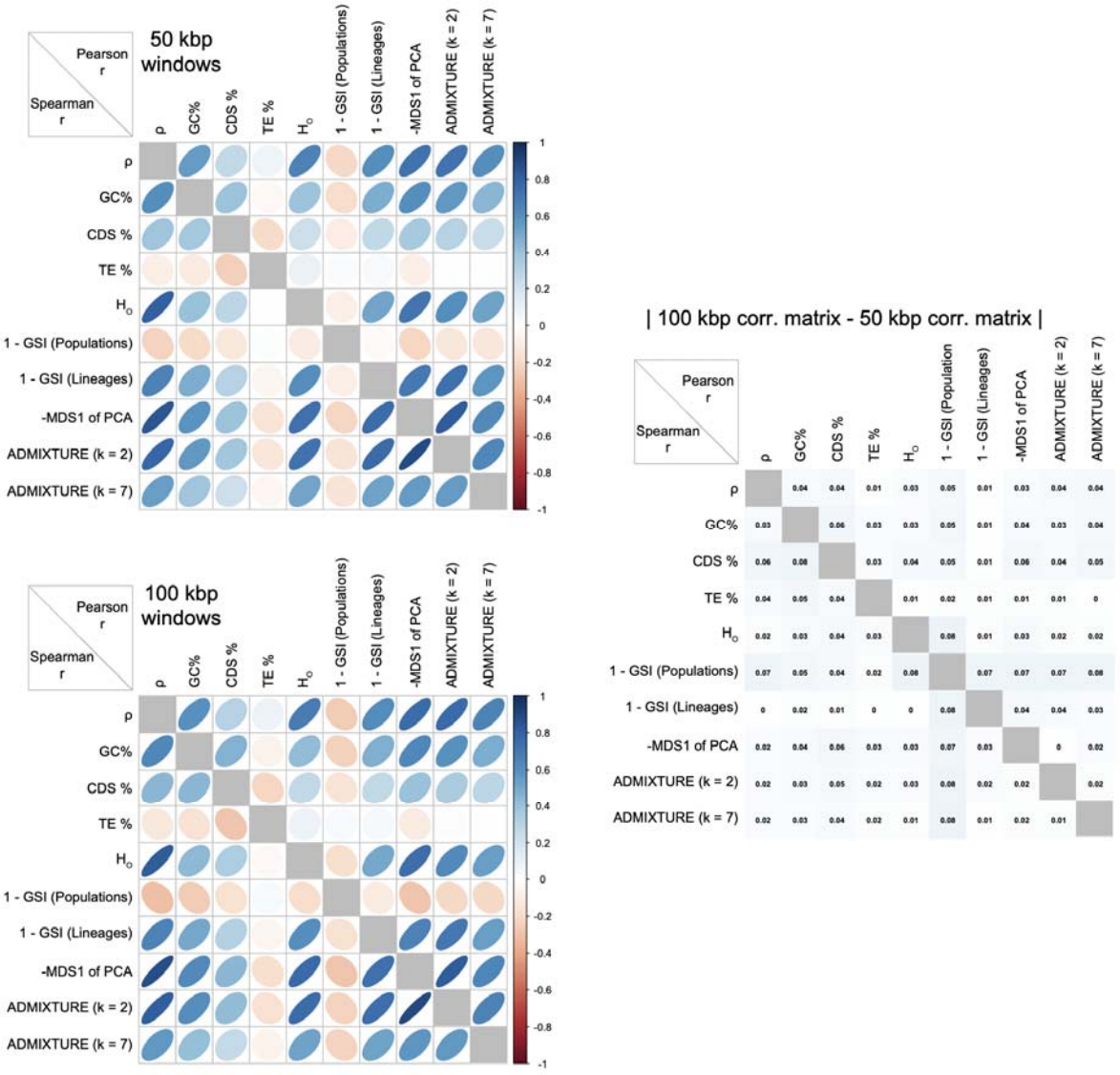

Figure S5. Demographic history estimated with MSMC2 for each individual. Thick lines indicate the whole genome estimate and thin lines indicate results from ten bootstrap replicates. Sample numbers correspond with those reported in Table S1.

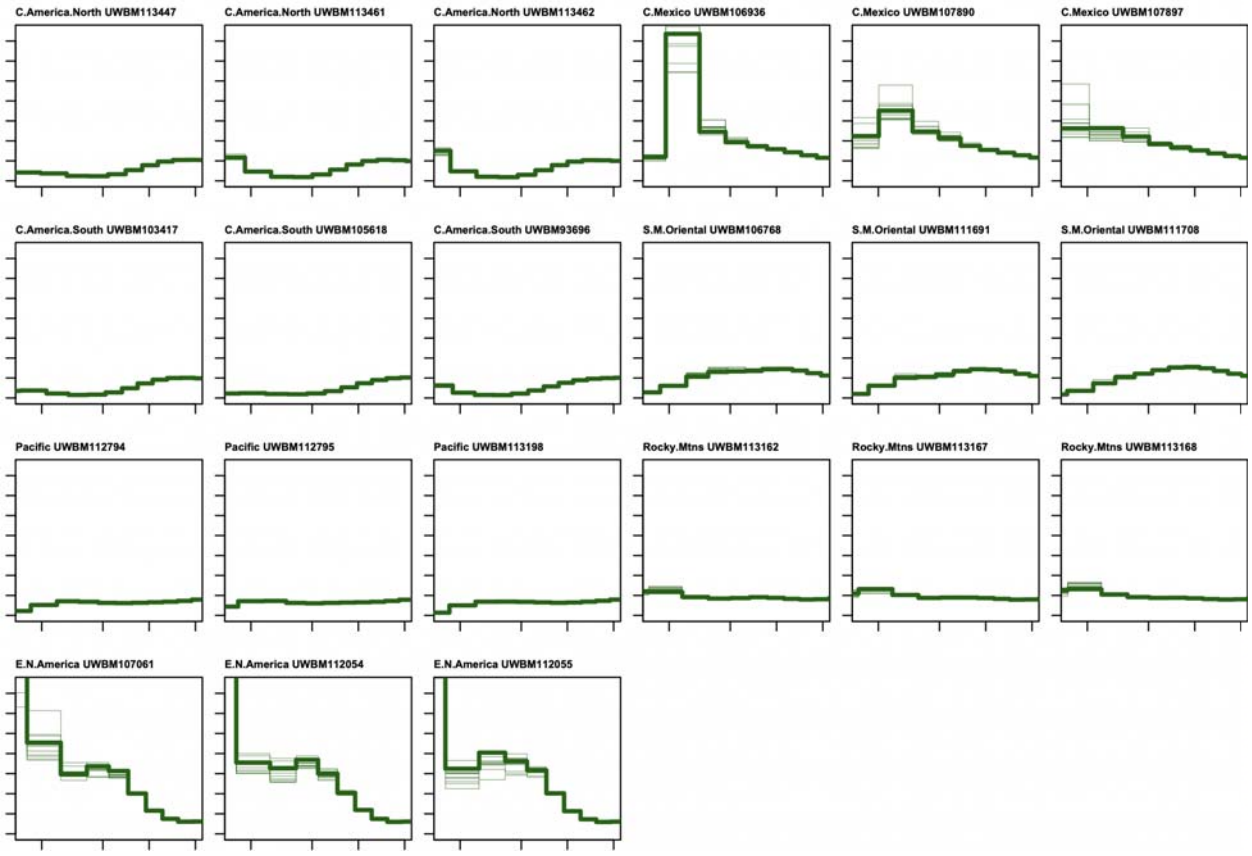

Figure S6. Violin plots of evolutionary rates (as measured by relative root-to-tip distances) for each population in the upper and lower genomic quintiles of high or low recombination (rho) values.

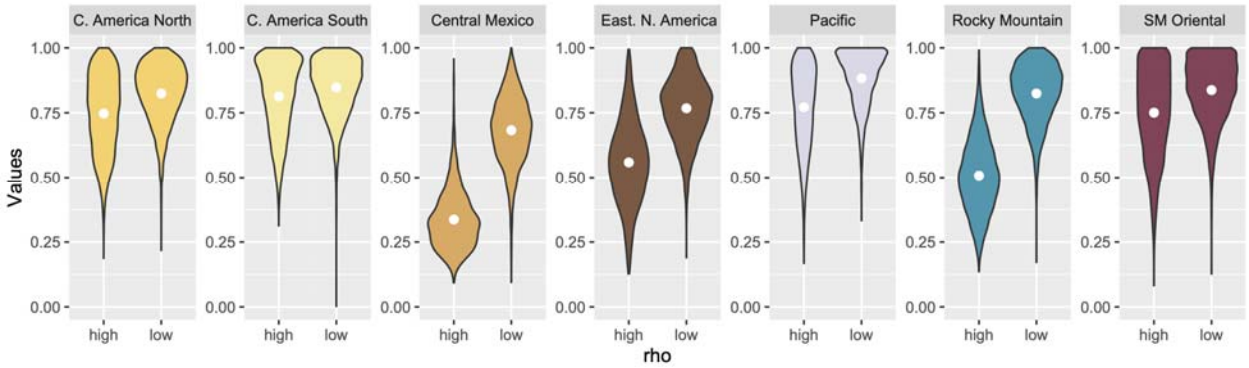

728 **LITERATURE CITED**

729

730 Alexander, D.H., Novembre, J., Lange, K., 2009. Fast model-based estimation of ancestry in
731 unrelated individuals. Genome Res. 19, 1655-1664.
732 Allmon, W.D., 1992. A causal analysis of stages in allopatric speciation. Oxford Surveys in
733 Evolutionary Biology 8, 219-219.
734 Bushnell, B., 2014. BBMap: A Fast, Accurate, Splice-Aware Aligner. Ernest Orlando Lawrence
735 Berkeley National Laboratory, Berkeley, CA (US).
736 Cantarel, B.L., Korf, I., Robb, S.M., Parra, G., Ross, E., Moore, B., Holt, C., Alvarado, A.S.,
737 Yandell, M., 2008. MAKER: an easy-to-use annotation pipeline designed for emerging
738 model organism genomes. Genome Res. 18, 188-196.
739 Cruickshank, T.E., Hahn, M.W., 2014. Reanalysis suggests that genomic islands of speciation
740 are due to reduced diversity, not reduced gene flow. Mol. Ecol. 23, 3133-3157.
741 Cummings, M.P., Neel, M.C., Shaw, K.L., 2008. A genealogical approach to quantifying lineage
742 divergence. Evolution 62, 2411-2422.
743 Danecek, P., Auton, A., Abecasis, G., Albers, C.A., Banks, E., DePristo, M.A., Handsaker, R.E.,
744 Lunter, G., Marth, G.T., Sherry, S.T., 2011. The variant call format and VCFtools.
745 Bioinformatics 27, 2156-2158.
746 Dutoit, L., Burri, R., Nater, A., Mugal, C.F., Ellegren, H., 2017. Genomic distribution and
747 estimation of nucleotide diversity in natural populations: perspectives from the collared
748 flycatcher (Ficedula albicollis) genome. Mol. Ecol. Res. 17, 586-597.
749 Edelman, N.B., Frandsen, P.B., Miyagi, M., Clavijo, B., Davey, J., Dikow, R.B., García-
750 Accinelli, G., Van Belleghem, S.M., Patterson, N., Neafsey, D.E., 2019. Genomic
751 architecture and introgression shape a butterfly radiation. Science 366, 594-599.
752 Ellegren, H., 2010. Evolutionary stasis: the stable chromosomes of birds. Trends Ecol. Evol. 25,
753 283-291.
754 Ellegren, H., Smeds, L., Burri, R., Olason, P.I., Backström, N., Kawakami, T., Künstner, A.,
755 Mäkinen, H., Nadachowska-Brzyska, K., Qvarnström, A., 2012. The genomic landscape
756 of species divergence in Ficedula flycatchers. Nature 491, 756.
757 Fontaine, M.C., Pease, J.B., Steele, A., Waterhouse, R.M., Neafsey, D.E., Sharakhov, I.V., Jiang,
758 X., Hall, A.B., Catteruccia, F., Kakani, E., 2015. Extensive introgression in a malaria
759 vector species complex revealed by phylogenomics. Science 347, 1258524.
760 Haenel, Q., Laurentino, T.G., Roesti, M., Berner, D., 2018. Meta□analysis of
761 chromosome□scale crossover rate variation in eukaryotes and its significance to
762 evolutionary genomics. Mol. Ecol. 27, 2477-2497.
763 Hale, M.C., Campbell, M.A., McKinney, G.J., 2021. A candidate chromosome inversion in
764 Arctic charr (*Salvelinus alpinus*) identified by population genetic analysis techniques. G3
765 11, jkab267.
766 Harrell, F.E., Dupont, C., 2020. Hmisc: Harrell Miscellaneous. R, R.
767 Hey, J., Kliman, R.M., 2002. Interactions between natural selection, recombination and gene
768 density in the genes of Drosophila. Genetics 160, 595-608.
769 Huang, K., Andrew, R.L., Owens, G.L., Ostevik, K.L., Rieseberg, L.H., 2020. Multiple
770 chromosomal inversions contribute to adaptive divergence of a dune sunflower ecotype.
771 Mol. Ecol. 29, 2535-2549.

Kapusta, A., Suh, A., 2017. Evolution of bird genomes—a transposon's□eye view. Ann. N. Y. Acad. Sci. 1389, 164-185.

Kawakami, T., Smeds, L., Backström, N., Husby, A., Qvarnström, A., Mugal, C.F., Olason, P., Ellegren, H., 2014. A high□density linkage map enables a second□generation collared flycatcher genome assembly and reveals the patterns of avian recombination rate variation and chromosomal evolution. Mol. Ecol. 23, 4035-4058.

Koonin, E.V., 2009. Evolution of genome architecture. The International Journal of Biochemistry & Cell Biology 41, 298-306.

Kulathinal, R.J., Bennett, S.M., Fitzpatrick, C.L., Noor, M.A., 2008. Fine-scale mapping of recombination rate in *Drosophila* refines its correlation to diversity and divergence. Proc. Natl. Acad. Sci. USA 105, 10051-10056.

Lanfear, R., Kokko, H., Eyre-Walker, A., 2014. Population size and the rate of evolution. Trends Ecol. Evol. 29, 33-41.

Li, G., Figueiró, H.V., Eizirik, E., Murphy, W.J., 2019. Recombination-aware phylogenomics reveals the structured genomic landscape of hybridizing cat species. Mol. Biol. Evol. 36, 2111-2126.

Li, H., Durbin, R., 2009. Fast and accurate short read alignment with Burrows–Wheeler transform. Bioinformatics 25, 1754-1760.

Li, H., Handsaker, B., Wysoker, A., Fennell, T., Ruan, J., Homer, N., Marth, G., Abecasis, G., Durbin, R., 2009. The sequence alignment/map format and SAMtools. Bioinformatics 25, 2078-2079.

Li, H., Ralph, P., 2019. Local PCA shows how the effect of population structure differs along the genome. Genetics 211, 289-304.

Linck, E., Battey, C., 2019. Minor allele frequency thresholds strongly affect population structure inference with genomic data sets. Mol. Ecol. Res. 19, 639-647.

Louis, M., Galimberti, M., Archer, F., Berrow, S., Brownlow, A., Fallon, R., Nykänen, M., O'brien, J., Robertson, K.M., Rosel, P.E., 2020. Selection on ancestral genetic variation fuels parallel ecotype formation in bottlenose dolphins. hal-03020428.

Lucas, T., 2016. palettetown: Use Pokemon Inspired Colour Palettes. R package version 0.1.1. https://CRAN.R-project.org/package=palettetown.

Manthey, J.D., Bourgeois, Y., Meheretu, Y., Boissinot, S., 2022. Varied diversification patterns and distinct demographic trajectories in Ethiopian montane forest bird (Aves: Passeriformes) populations separated by the Great Rift Valley. doi: 10.1111/mec.16417. Mol. Ecol.

Manthey, J.D., Klicka, J., Spellman, G.M., 2011a. Cryptic diversity in a widespread North American songbird: phylogeography of the Brown Creeper (Certhia americana). Mol. Phylogen. Evol. 58, 502-512.

Manthey, J.D., Klicka, J., Spellman, G.M., 2011b. Isolation□driven divergence: speciation in a widespread North American songbird (Aves: Certhiidae). Mol. Ecol. 20, 4371-4384.

Manthey, J.D., Klicka, J., Spellman, G.M., 2015. Chromosomal patterns of diversity and differentiation in creepers: a next-gen phylogeographic investigation of *Certhia americana*. Heredity 115, 165-172.

Manthey, J.D., Klicka, J., Spellman, G.M., 2021. The genomic signature of allopatric speciation in a songbird is shaped by genome architecture (Aves: *Certhia americana*). Genome Biol. Evol. 13, evab120.

817 Martin, S.H., Davey, J.W., Salazar, C., Jiggins, C.D., 2019. Recombination rate variation shapes
818 barriers to introgression across butterfly genomes. PLoS Biol. 17, e2006288.
819 Mayr, E., Mayr, E., Mayr, E., Mayr, E., 1963. Animal species and evolution. Belknap Press of
820 Harvard University Press Cambridge, Massachusetts.
821 McKenna, A., Hanna, M., Banks, E., Sivachenko, A., Cibulskis, K., Kernytsky, A., Garimella,
822 K., Altshuler, D., Gabriel, S., Daly, M., 2010. The Genome Analysis Toolkit: a
823 MapReduce framework for analyzing next-generation DNA sequencing data. Genome
824 Res. 20, 1297-1303.
825 McVean, G., Auton, A., 2007. LDhat 2.1: A package for the population genetic analysis of
826 recombination. Department of Statistics, Oxford, OX1 3TG, UK.
827 Mérot, C., Berdan, E.L., Cayuela, H., Djambazian, H., Ferchaud, A.-L., Laporte, M.,
828 Normandeau, E., Ragoussis, J., Wellenreuther, M., Bernatchez, L., 2021. Locally
829 adaptive inversions modulate genetic variation at different geographic scales in a
830 seaweed fly. Mol. Biol. Evol. 38, 3953-3971.
831 Moreira, L.R., Klicka, J., Smith, B.T., 2023. Demography and linked selection interact to shape
832 the genomic landscape of codistributed woodpeckers during the Ice Age. Mol. Ecol.,
833 DOI: 10.1111/mec.16841.
834 Nachman, M.W., Payseur, B.A., 2012. Recombination rate variation and speciation: theoretical
835 predictions and empirical results from rabbits and mice. Philosophical Transactions of the
836 Royal Society B: Biological Sciences 367, 409-421.
837 Nadachowska-Brzyska, K., Li, C., Smeds, L., Zhang, G., Ellegren, H., 2015. Temporal dynamics
838 of avian populations during Pleistocene revealed by whole-genome sequences. Curr.
839 Biol. 25, 1375-1380.
840 Neuwirth, E., 2014. RColorBrewer: ColorBrewer Palettes. R package version 1.1-2.
841 https://CRAN.R-project.org/package=RColorBrewer.
842 Nosil, P., Feder, J.L., 2012. Genomic divergence during speciation: causes and consequences.
843 Philosophical Transactions of the Royal Society of London B: Biological Sciences 367,
844 332-342.
845 Oksanen, J., Kindt, R., Legendre, P., O'Hara, B., Stevens, M.H.H., Oksanen, M.J., Suggests, M.,
846 2007. The vegan package. Community Ecology Package 10, 631-637.
847 Pagès, H., Aboyoun, P., Gentleman, R., DebRoy, S., 2017. Biostrings: Efficient manipulation of
848 biological strings. R Package Version 2.0.
849 Paradis, E., Claude, J., Strimmer, K., 2004. APE: analyses of phylogenetics and evolution in R
850 language. Bioinformatics 20, 289-290.
851 Perrier, C., Rougemont, Q., Charmantier, A., 2020. Demographic history and genomics of local
852 adaptation in blue tit populations. Evolutionary Applications 13, 1145-1165.
853 Poulin, J., D'Astous, É., Villard, M., Hejl, S., Newlon, K., McFadzen, M., Young, J., Ghalambor,
854 C., 2020. Brown Creeper (Certhia americana), version 1.0. In Birds of the World. . In:
855 Poole, A. (Ed.). Cornell Lab of Ornithology, Ithaca, NY, USA.
856 https://doi.org/10.2173/bow.brncre.01.
857 Ravinet, M., Yoshida, K., Shigenobu, S., Toyoda, A., Fujiyama, A., Kitano, J., 2018. The
858 genomic landscape at a late stage of stickleback speciation: High genomic divergence
859 interspersed by small localized regions of introgression. PLoS Genet. 14, e1007358.
860 Revell, L.J., 2012. phytools: an R package for phylogenetic comparative biology (and other
861 things). Methods Ecol. Evol. 3, 217-223.

Roesti, M., Moser, D., Berner, D., 2013. Recombination in the threespine stickleback genome—patterns and consequences. Mol. Ecol. 22, 3014-3027.

Sayyari, E., Mirarab, S., 2016. Fast coalescent-based computation of local branch support from quartet frequencies. Mol. Biol. Evol. 33, 1654-1668.

Schiffels, S., Durbin, R., 2014. Inferring human population size and separation history from multiple genome sequences. Nat. Genet. 46, 919.

Shi, Y., Bouska, K.L., McKinney, G.J., Dokai, W., Bartels, A., McPhee, M.V., Larson, W.A., 2021. Gene flow influences the genomic architecture of local adaptation in six riverine fish species. BioRxiv, DOI: https://doi.org/10.1101/2021.1105.1118.444736.

Singhal, S., Leffler, E.M., Sannareddy, K., Turner, I., Venn, O., Hooper, D.M., Strand, A.I., Li, Q., Raney, B., Balakrishnan, C.N., Griffith, S.C., McVean, G., Przeworski, M., 2015. Stable recombination hotspots in birds. Science 350, 928-932.

Smit, A., Hubley, R., Green, P., 2015. RepeatMasker Open-4.0. 2013–2015. Institute for Systems Biology. http://repeatmasker. org.

Stamatakis, A., 2014. RAxML version 8: a tool for phylogenetic analysis and post-analysis of large phylogenies. Bioinformatics 30, 1312-1313.

Stankowski, S., Chase, M.A., Fuiten, A.M., Rodrigues, M.F., Ralph, P.L., Streisfeld, M.A., 2019. Widespread selection and gene flow shape the genomic landscape during a radiation of monkeyflowers. PLoS Biol. 17, e3000391.

Sukumaran, J., Holder, M.T., 2010. DendroPy: a Python library for phylogenetic computing. Bioinformatics 26, 1569-1571.

Tacutu, R., Thornton, D., Johnson, E., Budovsky, A., Barardo, D., Craig, T., Diana, E., Lehmann, G., Toren, D., Wang, J., 2017. Human Ageing Genomic Resources: new and updated databases. Nucleic Acids Res. 46, D1083-D1090.

Thom, G., Moreira, L.R., Batista, R., Gehara, M., Aleixo, A., Smith, B.T., 2024. Genomic architecture predicts tree topology, population structuring, and demographic history in Amazonian birds. Genome Biol. Evol., evae002.

Tigano, A., Khan, R., Omer, A.D., Weisz, D., Dudchenko, O., Multani, A.S., Pathak, S., Behringer, R.R., Aiden, E.L., Fisher, H., 2021. Chromosome size affects sequence divergence between species through the interplay of recombination and selection. bioRxiv.

Todesco, M., Owens, G.L., Bercovich, N., Légaré, J.-S., Soudi, S., Burge, D.O., Huang, K., Ostevik, K.L., Drummond, E., Imerovski, I., 2020. Massive haplotypes underlie ecotypic differentiation in sunflowers. Nature 584, 602-607.

Toews, D.P., Taylor, S.A., Vallender, R., Brelsford, A., Butcher, B.G., Messer, P.W., Lovette, I.J., 2016. Plumage genes and little else distinguish the genomes of hybridizing warblers. Curr. Biol. 26, 2313-2318.

Vijay, N., Bossu, C.M., Poelstra, J.W., Weissensteiner, M.H., Suh, A., Kryukov, A.P., Wolf, J.B., 2016. Evolution of heterogeneous genome differentiation across multiple contact zones in a crow species complex. Nat. Comm. 7, 1-10.

Wei, T., Simko, V., Levy, M., Xie, Y., Jin, Y., Zemla, J., 2017. Package 'corrplot'. Statistician 56, e24.

Whiting, J.R., Paris, J.R., van der Zee, M.J., Parsons, P.J., Weigel, D., Fraser, B.A., 2021. Drainage-structuring of ancestral variation and a common functional pathway shape limited genomic convergence in natural high-and low-predation guppies. PLoS Genet. 17, e1009566.

908 Wickham, H., 2011. ggplot2. Wiley Interdisciplinary Reviews: Computational Statistics 3, 180-
909 185.
910 Wu, C.I., 2001. The genic view of the process of speciation. J. Evol. Biol. 14, 851-865.
911 Zhang, C., Rabiee, M., Sayyari, E., Mirarab, S., 2018. ASTRAL-III: polynomial time species
912 tree reconstruction from partially resolved gene trees. BMC Bioinformatics 19, 153.
913